



HAL
open science

Engineering 3D micro-compartments for highly efficient and scale-independent expansion of human pluripotent stem cells in bioreactors

Philippe J.R. Cohen, Elisa Luquet, Justine Pletenka, Andrea Leonard, Elise Warter, Basile Gurchenkov, Jessica Carrere, Clément Rieu, Jerome Hardouin, Fabien Moncaubeig, et al.

► To cite this version:

Philippe J.R. Cohen, Elisa Luquet, Justine Pletenka, Andrea Leonard, Elise Warter, et al.. Engineering 3D micro-compartments for highly efficient and scale-independent expansion of human pluripotent stem cells in bioreactors. *Biomaterials*, 2023, 295, pp.122033. 10.1016/j.biomaterials.2023.122033 . hal-04089924

HAL Id: hal-04089924

<https://u-paris.hal.science/hal-04089924>

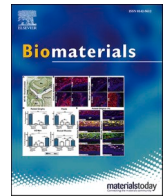
Submitted on 5 May 2023

HAL is a multi-disciplinary open access archive for the deposit and dissemination of scientific research documents, whether they are published or not. The documents may come from teaching and research institutions in France or abroad, or from public or private research centers.

L'archive ouverte pluridisciplinaire **HAL**, est destinée au dépôt et à la diffusion de documents scientifiques de niveau recherche, publiés ou non, émanant des établissements d'enseignement et de recherche français ou étrangers, des laboratoires publics ou privés.



Distributed under a Creative Commons Attribution - NonCommercial - NoDerivatives 4.0 International License



Engineering 3D micro-compartments for highly efficient and scale-independent expansion of human pluripotent stem cells in bioreactors

Philippe J.R. Cohen^{a,b,*}, Elisa Luquet^b, Justine Pletenka^b, Andrea Leonard^b, Elise Warter^b, Basile Gurchenkov^c, Jessica Carrere^b, Clément Rieu^b, Jerome Hardouin^b, Fabien Moncaubeig^b, Michael Lanero^b, Eddy Quelebec^{a,b}, Helene Wurtz^b, Emilie Jamet^b, Maelle Demarco^b, Celine Banal^a, Paul Van Liedekerke^d, Pierre Nassoy^{e,f}, Maxime Feyeux^b, Nathalie Lefort^{a,1}, Kevin Alessandri^{b,1}

^a Université Paris Cité, Imagine Institute, IPSC Core Facility, INSERM UMR U1163, F-75015, Paris, France

^b Treefrog Therapeutics, F-33600, Pessac, France

^c Paris Brain Institute, ICM Paris, F-75013, Paris, France

^d Inria Paris & Sorbonne Université LJLL, 2 Rue Simone IFF, F-75012, Paris, France

^e LP2N, Laboratoire Photonique Numérique et Nanosciences, Univ. Bordeaux, F-33400, Talence, France

^f Institut D'Optique Graduate School & CNRS UMR 5298, F-33400, Talence, France

ARTICLE INFO

Keywords:

Human induced pluripotent stem cells
3D culture
Cell expansion
Stem cell niche
Biomicrofluidics

ABSTRACT

Human pluripotent stem cells (hPSCs) have emerged as the most promising cellular source for cell therapies. To overcome the scale-up limitations of classical 2D culture systems, suspension cultures have been developed to meet the need for large-scale culture in regenerative medicine. Despite constant improvements, current protocols that use microcarriers or generate cell aggregates only achieve moderate amplification performance. Here, guided by reports showing that hPSCs can self-organize *in vitro* into cysts reminiscent of the epiblast stage in embryo development, we developed a physio-mimetic approach for hPSC culture. We engineered stem cell niche microenvironments inside microfluidics-assisted core-shell microcapsules. We demonstrate that lumenized three-dimensional colonies significantly improve viability and expansion rates while maintaining pluripotency compared to standard hPSC culture platforms such as 2D cultures, microcarriers, and aggregates. By further tuning capsule size and culture conditions, we scale up this method to industrial-scale stirred tank bioreactors and achieve an unprecedented hPSC amplification rate of 277-fold in 6.5 days. In brief, our findings indicate that our 3D culture system offers a suitable strategy both for basic stem cell biology experiments and for clinical applications.

1. Introduction

Therapeutic cells represent hope for millions of patients worldwide with chronic diseases or unmet medical needs. For each of those patients, the number of required cells ranges between 10^5 and 10^{10} cells. While academic pre-clinical studies or small-scale clinical trials have already been proven to be successful [1,2], a transition to a true clinical scale is now urgently needed. To enable the treatment of thousands to millions of patients, production capacity must scale while maintaining high-quality cells compatible with transplantation.

Due to their unlimited self-renewal capacity and potency to give rise to any cell type in the body, human pluripotent stem cells (hPSCs) hold great promise to provide the required quantities of therapeutic cells. *In vivo*, a few embryonic stem cells can give rise to the 30×10^{12} cells of the adult human body while maintaining their genome integrity. Consequently, much effort has been dedicated to the isolation and *in vitro* culture of these cells in physiological conditions.

Historically, the first stem cell lines were established by micro-dissecting embryos and manual passaging as two-dimensional (2D) adherent epithelial colonies on a layer of feeder cells [3]. Cell

* Corresponding author. Université Paris Cité, Imagine Institute, IPSC Core Facility, INSERM UMR U1163, F-75015, Paris, France.

E-mail address: philippe.cohen@outlook.com (P.J.R. Cohen).

¹ These authors contributed equally to this work.

proliferation and pluripotency maintenance were thus achieved *in vitro*. The need for an embryonic source was then alleviated with the discovery that differentiated cells could be reprogrammed into induced pluripotent stem cells (iPSC) [4]. This breakthrough led to the pioneer works in developmental cell biology and catalyzed the development of cell therapy applications. Even though much work has been devoted to the development of media and substrate compatible with clinical use, the topology of hiPSCs cultures, which fail to preserve the desired three-dimensional (3D) architecture of the early embryonic micro-environment, remains a severe limitation. Indeed, 2D *in vitro* cultures suffer high mortality rates, spontaneous differentiation, and genetic drift [2]. An estimated 40-fold increase in the number of mutations compared to *in vivo* conditions [5] often results in the rejection of clinical batches due to safety concerns [6,7]. Moreover, 2D culture systems have limited “scale-out” (i.e. parallelization) possibilities: for example, generating 1 trillion pluripotent stem cells would require almost 1000 m² of plastic dishes and countless handmade passaging [2]. In addition to batch-to-batch variability and lack of process control, this non-scalability remains the main limitation of 2D culture systems for clinical applications [7].

More recently, 3D hPSCs cultures have been developed to model developmental processes. After seeding PSCs in bulk extracellular matrix (ECM) [8,9] or using microfluidic chips [10], cell clusters self-organize into a monolayered epithelium recapitulating several features of an epiblast in embryo development [11,12]. Even though these elegant approaches allowed to gain much insight into morphogenesis mechanisms [13], they remain small-scale and are thus not designed for hPSCs expansion and bioprocessing per se.

From a bioproduction perspective, significant advances have been achieved in the last two decades. The ability to grow hPSCs as floating aggregates or adherent at the surface of microcarriers inherently provides increased surface-to-volume ratio and scale-up potentialities. However, the pioneering works from Zandstra and colleagues demonstrated that the growth of embryoid bodies derived from embryonic stem cells was inhibited by uncontrolled agglomeration, while culture after embedding cells in agarose droplets lifts this limitation and is amenable to scalable production of embryonic cells in stirred suspension culture [14,15]. The use of stirred-tank bioreactors (STBR) has become crucial in most bioproduction strategies because they allow better control of the culture parameters without direct human intervention. Indeed, stirring-mediated mechanical agitation avoids sedimentation of the aggregates or microcarriers onto the bottom of the culture vessel and heterogeneities in the culture medium compositions. Nonetheless, one intrinsic drawback of agitation is that hydrodynamic shear induces cellular damage [16]. Even though expansion rates with hPSC aggregates are regularly increased and could reach up to 70-fold within 7 days [17,18], the ability to scale up the production volume is still restricted. Typically, this mechanical upper limit makes it challenging to reach batches larger than 1 L or equivalently few billion cells. Finally, one of the key bottlenecks for industrial scalability is the difficulty of simultaneously fulfilling high fold expansion, large volume, and physiological quality [19–21].

In this work, we show that the design of engineered ECM-laden hPSC micro-environments allows to optimize the suspension culture of hPSC in STBRs. More precisely, we propose a system that utilizes a high throughput microfluidic encapsulation technology compatible with suspension culture of stem cells in a bioreactor and amenable to the production of large volume batches without any compromise on cell survival in contrast with 2D colony-based systems, which generally suffer from low viability passaging or harvesting [2,22]. Briefly, iPSCs are encapsulated in alginate hollow microcapsules internally coated with ECM components at low cell seeding concentration. We assess the maintenance of stemness and pluripotency upon 3D culture in suspension. We then characterize the cell growth inside the capsules before showing that upscaling to 10 L-STBR allows to reach unrivalled unrivalled amplification factors. Altogether, the proposed technology

overcomes the scale-up bottleneck faced in cell therapy bioproduction. We discuss that this performance could be due to our ability to recapitulate *in capsulo* a 3D lumenized colony that morphologically resembles an epiblast rosette, and which has higher cell viability than 2D colonies and microcarrier or aggregate systems.

2. Results

2.1. High-throughput microfluidic encapsulation allows the expansion of hiPSCs in 3D lumenized colonies

Using a microfluidic technique to generate hollow hydrogel spheres (Fig. 1A, Movie S1, and detailed description in the Methods section) previously developed by us and others [23–26], we encapsulated hiPSCs in liquid core capsules. Our routine protocol produces capsules at a rate of about 3 kHz (Fig. S1), meaning that a 30 s operation generates 100,000 capsules. Morphological analysis shows that capsules are monodisperse in size with mean external radius $R = 205 \mu\text{m} \pm 39 \mu\text{m}$ and that their shape is close to spherical, with a circularity parameter $C = 0.84 \pm 0.04$, $n = 125$ (Fig. 1B). This size, which is below the distance over which oxygen and nutrients supply is limited within a tissue, allows to avoid the formation of a necrotic core [27].

Supplementary data related to this article can be found at <https://doi.org/10.1016/j.biomaterials.2023.122033>.

To provide a niche-like environment to hiPSCs, Matrigel, an ECM mixture, is co-injected with the cell suspension [25]. Empirically, we found that a minimal volume fraction of 25% was required to form a continuous matrix layer anchored to the inner wall of the capsule, with the excess (if any) being found as floating gel pieces inside the capsule [26]. Most of the experiments reported in these works were performed with 50% of Matrigel in volume fraction. The granularity seen in the core of the capsule (Fig. 1E) thus corresponds to small floating aggregates of ECM. Most encapsulations reported hereafter were performed with a density of 0.4×10^6 cells/mL in the cell/matrix suspension, unless otherwise stated, and led to a mean number of cells per capsule right after encapsulation (day 0) of ~ 2.5 (Fig. 1C), meaning that $\sim 10\%$ of the capsules are empty, consistently with a Poisson distribution. After 6–7 days of culture, practically defined as the harvest time under these seeding conditions, 3D colonies of hiPSCs were observed, suggesting not only that hiPSCs survive but also that they could proliferate (Fig. 1D). Higher magnification reveals the presence of a lumen (Fig. 1E).

2.2. Encapsulated 3D hiPSC colonies self-organize, grow and maintain stemness

Using phase contrast imaging, we observed the growth kinetics of these 3D hiPSC colonies in greater detail. First, hiPSCs form a small cluster (typically during the first 24 h) before self-organizing in a cyst structure around a central lumen (Fig. 2A, Movie S2 & S3). Then, the 3D hiPSC colonies grow within the capsules while keeping the same spherical shape. In the early stages, the cells within the monolayer of the cyst have a cuboid cell shape of about $10 \mu\text{m}$ side (Fig. 2B left, ~ 5 days post-encapsulation). Before harvesting, as seen in the confocal image of a representative 7-day-old hiPSC 3D colony immunostained for actin and nucleus, cells exhibit an elongated morphology perpendicular to the surface of the cyst. Yet, the cyst remains monolayered, suggesting a transition towards a pseudostratified columnar epithelium with most nuclei located on the basal side opposing the lumen. In this stage, the cysts are characterized by a thickness of about $\sim 40 \mu\text{m}$ (Fig. 2B right) and a radius of about $\sim 100 \mu\text{m}$ (Fig. S2, day 7). Note that later stages are ignored. Indeed, if cells are not harvested, cysts become confined by the capsules and further grow inwards, leading to a progressive loss of the lumen (Movie S4) and eventually the appearance of “fractures” (Fig. S2).

Supplementary data related to this article can be found at <https://doi.org/10.1016/j.biomaterials.2023.122033>.

The maintenance of the stemness of the encapsulated 3D hiPSC

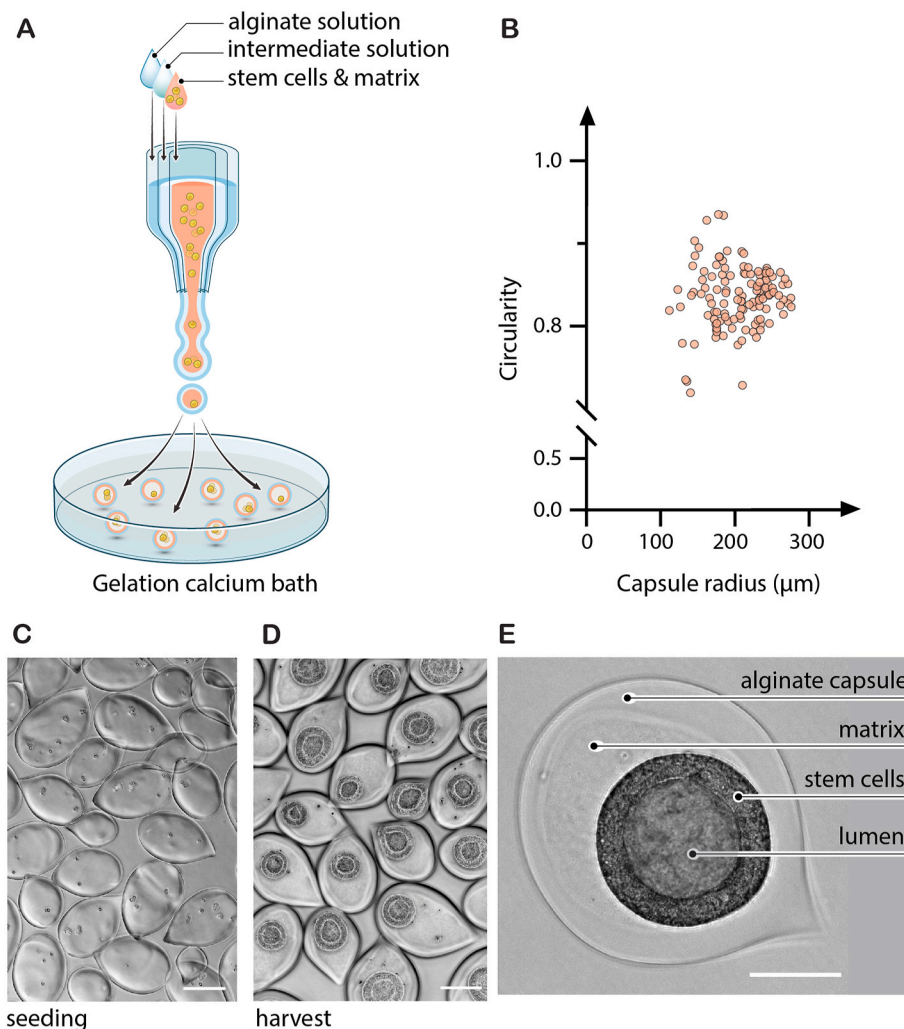


Fig. 1. Encapsulation of human pluripotent stem cells (hPSCs) and suspension culture of 3D lumenized colonies (A) Working principle of the microfluidic encapsulation technique. Co-extrusion of three co-axial flows generates composite cell-and extracellular matrix (ECM)-laden droplets. The outer layer composed of alginate solution undergoes gelation upon contact with a calcium bath. Cells are entrapped in the core-shell capsules and ECM condensates onto the internal wall to form a niche-like environment. (B) Morphometric analysis of the capsules. Graph of capsule circularity as a function of capsule radius for a representative batch of capsules ($n = 125$). (C-D) Phase contrast micrographs of the encapsulated hPSCs after seeding at day 0 (C) and before harvest at day 7 (D) of the suspension culture course. Scale bar is $200 \mu\text{m}$. (E) Magnified phase contrast image showing the hollow alginate capsule revealing the cyst architecture of the encapsulated hPSC colony. Scale bar = $100 \mu\text{m}$.

colonies was then checked. The expression of key self-renewal markers such as OCT4 and SOX2 was first assessed after capsule dissolution, fixation and staining. The alginate shell was dissolved while preserving the 3D architecture [25] (see Methods section). Image analysis of representative confocal images of individual cysts (Fig. 2C (top row) and Fig. S2) allows to derive that the percentage of cells positive for OCT4 and SOX2 is 97% (Fig. 2D top row). To further assess the consistency of stemness phenotype, we applied the approach pursued in a different context for epiblast-stage hPSCs spheroids by Freedman et al. [28]. “Naked” hiPSCs cysts were dissociated and replated into 2D cultures (Fig. 2C). We observed that 2D colonies are readily formed, and stemness markers are detected (Fig. 2C–D, bottom row) with a percentage of OCT4 and SOX2 positive cells larger than 98%.

Following this characterization at the scale of individual capsules, we sought to assess the potential variability between capsules and between hiPSC lines. We thus dissociated the bulk suspension cultures, extended staining to OCT4, SOX2 and NANOG and performed flow cytometry (Fig. 2E–F). For 4 different cell lines (see Methods section) by pooling all experiments ($n = 42$) of each hiPSC line, we found that the mean percentage of positive cells is 93% OCT4, 98% SOX2 or 92% NANOG (Fig. 2F). This finding is in good agreement with the above-described findings at the single 3D colony level, suggesting an overall homogeneity of the stem cell culture.

Note that, if the capsules culture was prolonged beyond 7 days, despite drastic changes of topology from cyst to aggregate (Fig. S2 C-E and Movie S4), the stemness of the hiPSCs was not affected, as revealed

by OCT4 and SOX2 staining before and after lumen collapse (Fig. S2 B-C), suggesting that harvest timing is not critically stringent with respect to the stemness maintenance.

2.3. Encapsulated 3D hiPSC colonies maintain pluripotency and genomic integrity

While OCT4, SOX2 and NANOG are often considered pluripotency markers, they actually are stemness markers. To assess the pluripotency more thoroughly and validate the quality of hPSCs upon 3D culture in their ability to differentiate as bona fide pluripotent stem cells, the trilineage differentiation assay is used in which stochastic differentiation is induced. Following a standard protocol (see Methods section), decapsulated and dissociated hiPSCs (from the three available cell lines) were driven towards early differentiation, as shown by the stainings for specific markers of the three germ layers (Fig. 3A). Even though the expression level may differ from one cell line to another, all stainings are positive and clearly reveal a differentiation into the three germ layers.

To further quantify the differentiation potential after 3D culture within capsules, we used qPCR Scorecard™ assay to evaluate the transcription profile of the cells obtained in the trilineage assay (Fig. 3B). The set of 94 previously validated qPCR markers of self-renewal, ectoderm, mesoderm, mesoderm and endoderm was used to compare standard 2D culture and 3D culture-in-capsules. Fig. 3B shows that, for a given marker and a given cell line, there is a similar gene expression pattern between the transcription signatures in 2D and 3D culture

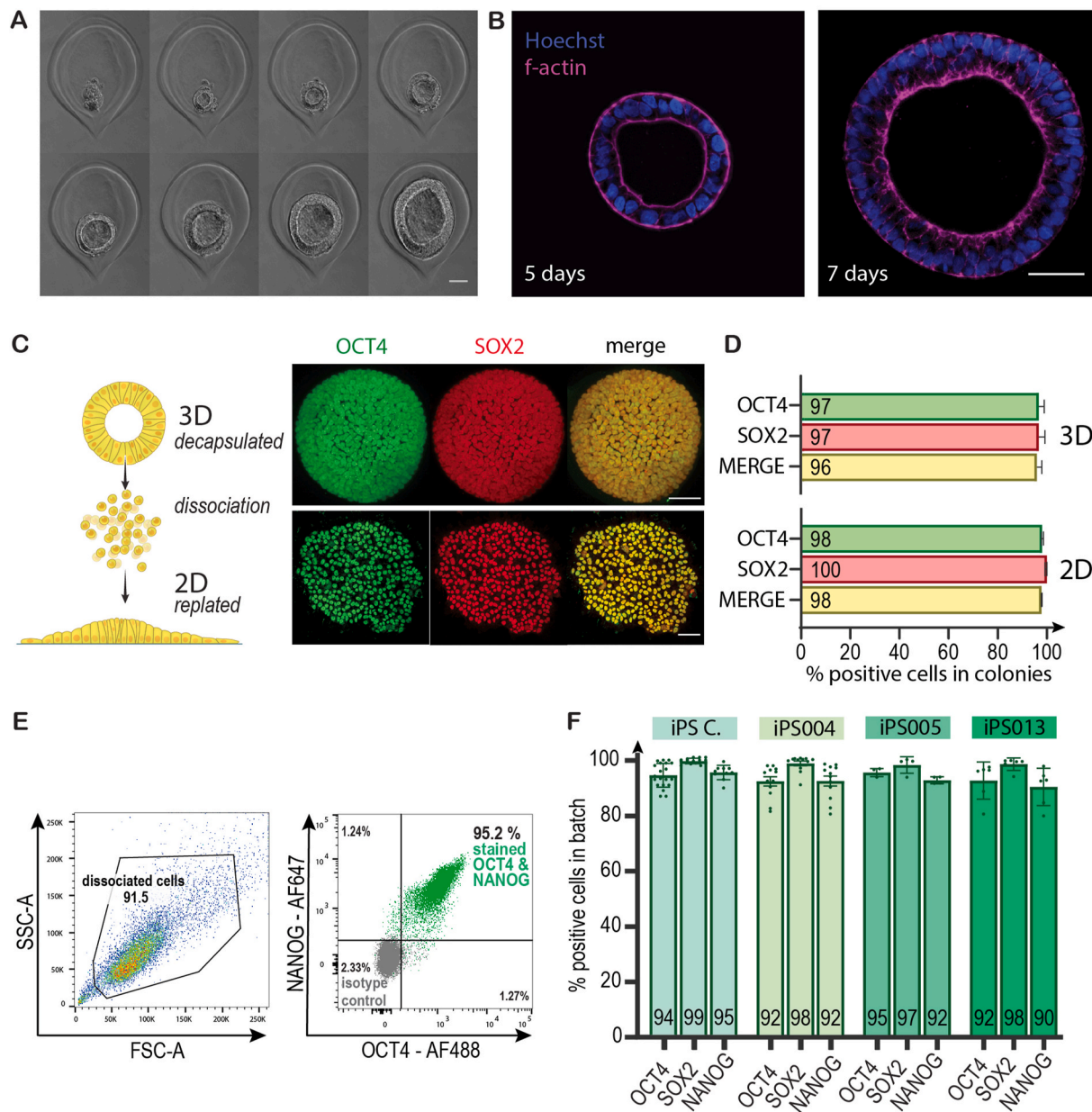


Fig. 2. Morphology, growth and stemness of *in capsulo* self-assembled 3D hPSC colonies (A) Snapshots of phase-contrast microscopy images showing the growth of an 3D hPSC colony. The time interval between successive images is 12 h. The first image was captured 24 h after encapsulation, just after first medium change and removal of rock inhibition. The scale bar is 50 μ m. (B) Confocal image of the equatorial plane of a hPSC colony grown in a capsule at day 5 (left) and day 7 (right) cytoskeletal actin is stained in purple (Phalloidin) and nuclei in blue (Hoechst). Scale bar = 50 μ m. (C) Left: Cartoon explaining how 3D hPSC colonies are dissociated and replated to form 2D colonies. Right: Immunostaining of a representative encapsulated 3D colony (upper panel, scale bar = 50 μ m) and a 2D colony obtained after replating (lower panel, scale bar = 100 μ m): OCT4 (green) SOX2 (red) and Merge (OCT4/SOX2). (D) Percentage of cells positive for markers of stemness among 4 representative colonies co-stained for OCT4 and SOX2 in 3D capsules (upper panel) and in 2D (lower panel). Number of counted nuclei: n = 1159 for 3D and n = 671 for 2D cells, see also Fig. S3). Error bars show the standard deviation of the mean. (E) Flow cytometry dot-plots for stemness markers (OCT4 and NANOG) of a batch of 3D hPSC colonies after 7 days of culture (T-flask). (F) Bar chart showing the percentage of OCT4, SOX2 or NANOG positive cells in 3D hPSC colonies (culture in T-flask) analyzed by flow cytometry at 7 days post encapsulation for 4 iPS cell lines (with n \geq 3 independent biological replicates per cell line, n = 42 total number of experiments). Error bars represent the standard error of the mean. (For interpretation of the references to colour in this figure legend, the reader is referred to the Web version of this article.)

conditions, indicating that pluripotency assessed as the *in vitro* differentiation capability of hiPSC colonies is definitely not altered in our encapsulated 3D colonies. A pooled analysis by germ layer (Fig. S4) confirms a similar differentiation profile between 2D and 3D stem cells.

Finally, to control the genomic integrity of the 3D colonies, we performed high-resolution SNP (single nucleotide polymorphism) arrays before and after amplification within the capsules (Fig. 3C and Fig. S5) [29]. Comparative SNP analysis showed the absence of aneuploidies,

deletions or duplications, as evidenced by the superimposable karyotypes. The high degree of SNP concordance (>99.8% for all hiPSC lines) before and after encapsulation confirms cell line identity (Fig. 3D).

Capsule-scale expansion of a3D hiPSC colony can be upscaled in static suspensions and bioreactors.

To evaluate whether the strategy to produce 3D colonies in ECM-coated capsules impacts the growth and expansion rates of hiPSC, we performed a series of systematic experiments to probe the cell growth

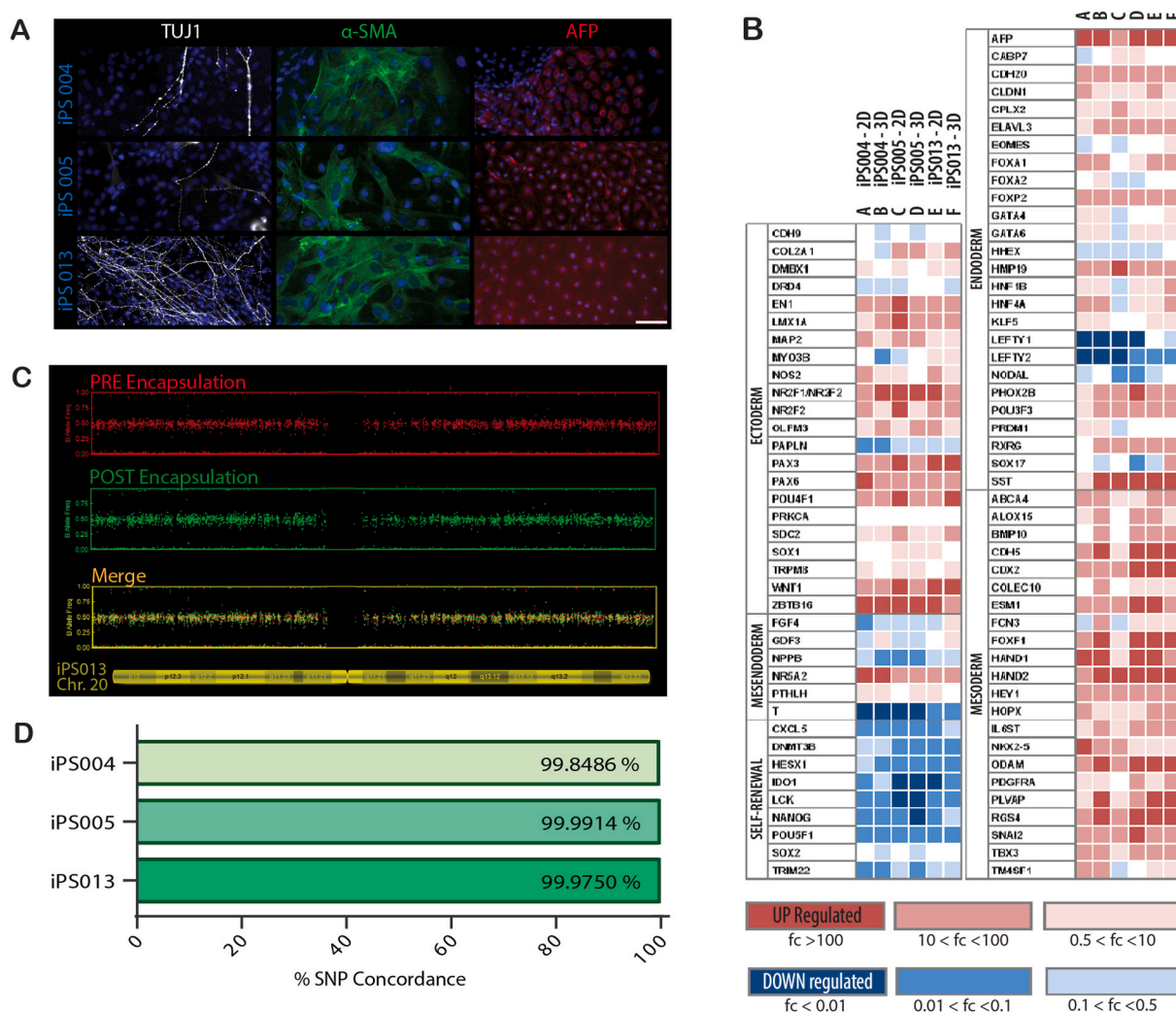


Fig. 3. Maintenance of pluripotency and genomic integrity in 3D hPSC colonies (A) Microscopy images of immunohistochemistry-based trilineage assay of 3 iPSC lines with 4 stainings: TUJ1 (white, early ectoderm), α -SMA (green, early mesoderm), AFP (Red, early endoderm), DAPI (Blue). (B) Scorecard™ differentiation assay comparing 3 iPSC cell lines expanded in 2D and 3D encapsulated hPSC colonies. (C) Comparison of high-resolution SNP arrays before and after one-week of encapsulation for iPS013 cell line: Zoom on chromosome 20 for pre-encapsulation (red) and post-encapsulation (green). The merge (yellow) is shown to highlight the absence of duplications and deletions. (D) Quantitative analysis yielding genotype SNP concordance before and after one-week of amplification as encapsulated 3D colonies for 3 cell lines. (For interpretation of the references to colour in this figure legend, the reader is referred to the Web version of this article.)

kinetics. The standard 2D cell cultures were taken as a control. To characterize the fold expansion rate, we define the amplification factor (AF) as $AF = N(t_0 + \Delta t) / N(t_0)$, where $N(t_0)$ and $N(t_0 + \Delta t)$ are the cell numbers at the initial time t_0 and $t_0 + \Delta t$ respectively, direct cell counting at day 6 after passaging give a mean $AF_{2D}(t = 6 \text{ days}) \sim 13$. Since, by definition, $AF(\Delta t) = 2^{\Delta t / PDT} = e^{(\ln 2 / PDT) \times \Delta t}$, with PDT the cell population doubling time, by fitting $AF(\Delta t)$ with an exponential function, we derive a mean $PDT_{2D} = 34 \text{ h} \pm 5 \text{ h}$ from the characteristic rising time for iPSC line, which falls within the range of data reported in the literature [2,4,30].

Then, in order to characterize the growth of individual encapsulated 3D hiPSC colonies, we cultured them in 35 mm Petri dishes (typically as few as 10 capsules in a volume of medium $\sim 5 \text{ mL}$, permitting to conserve the same medium for the whole course of the experiment without the risk of nutrient depletion and acidification). We performed time-lapse phase contrast imaging over one week. We assume that cell volume remains constant, which allows us to derive $AF_{\text{capsule}}(\Delta t) = V(t_0 + \Delta t) / V(t_0)$ by measuring the volume of the cyst $V(t)$ from image analysis: $V(t) = \frac{4\pi}{3}(R_{\text{out}}^3 - R_{\text{in}}^3)$, where R_{in} and R_{out} are the average internal and external radii of the cyst (see notations on Fig. 4A). Fig. 4B shows the evolution of AF_{capsule} as a function of time for individual

encapsulated 3D colonies. One immediately observes that $AF_{\text{capsule}}(t = 7 \text{ days}) = 212$. Additionally, since AF increases exponentially as $AF(\Delta t) = 2^{\Delta t / PDT}$, one finds $PDT_{\text{capsule}} = 22 \pm 1 \text{ h}$.

With the perspective of scaling up the production of hiPSCs, we also investigated how the growth of encapsulated 3D hiPSC colonies was impacted when cultured in conditions of i) static bulk suspension in standard T-flasks (Fig. 4B) and ii) stirred suspension in a benchtop bioreactor (Fig. 4C). STBRs are the most common bioreactors used to culture biological agents for biotechnological applications. Besides their capacity to monitor pH, oxygen partial pressure, and to refresh the medium, the mechanical agitation provided by the impellers allows better fluid mixing and oxygen transfer ability as compared to static suspension [31]. However, the drawback may also be that the shear stress induced by the impellers was shown to cause deleterious effects such as cell death or a decrease in cell growth in aggregate- or microcarrier-based cultures [32, 33]. Practically, we loaded capsules from the same batch in T-flasks and in a STBR at the same initial density. The bioreactor impeller rotational speed was set to 150 rpm, sufficient to perform efficient mixing, thus ensuring medium homogeneity and avoiding capsule sedimentation. We could not detect any change in the shape of the capsules and 3D colonies under these stirring conditions.

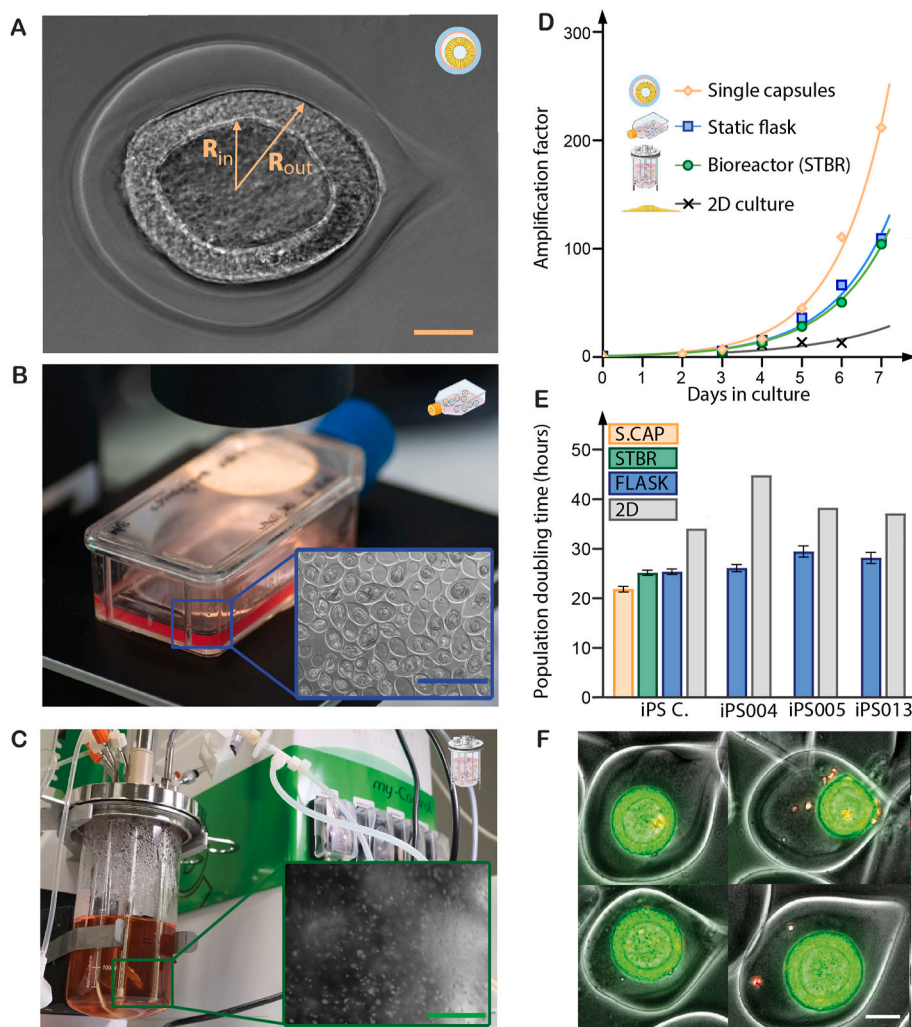


Fig. 4. Amplification of 3D hiPSC colonies at the scale of a single capsule, in a static suspension and in bioreactors (A) Micrograph of a 3D hiPSC colony in a capsule and notations used in the next for the internal and external radii of the cyst. (B) Static suspension culture of encapsulated 3D hiPSCs. Insert: Phase contrast image showing 3D hiPSCs colonies in capsules. Scale bar is 1000 μm . (C) Stirred suspension culture of encapsulated 3D hiPSCs in a 500 mL benchtop STBR. Insert: Picture of the flowing capsules in the bioreactor. Scale bar is 4 mm. (D) Amplification factor as a function of time for single capsules (orange, $n = 6$), static culture (blue, $n = 2$), stirred culture in a benchtop (volume 500 mL) bioreactor (green, $n = 2$), and conventional 2D cultures (grey, $n = 1$). Last points in the graph correspond to the harvest time. (E) Population doubling time of encapsulated hiPSC colonies in single capsules (S-CAP, orange, $n = 6$), in a flask (FLASK, blue, $n = 42$) and a benchtop bioreactor (STBR, green, $n = 2$) and in standard 2D cultures (2D, grey, $n = 1$ for each condition). Error bars represent the standard error of the mean. (F) Fluorescence microscopy image of 4 representative encapsulated 3D hiPSC colonies stained with Live/dead (green/red). Scale bar is 100 μm . All data shown here were obtained with iPS C line, except panel 4D which collects data for the 4 available cell lines. (For interpretation of the references to colour in this figure legend, the reader is referred to the Web version of this article.)

Then, after the dissolution of the alginate shell and dissociation of the cysts, we counted the stem cells in both static and stirred culture conditions to derive the AF at different time points. We found $AF_{\text{flask}}(7 \text{ days}) = 109 \pm 6$ and $AF_{\text{bioreactor}}(7 \text{ days}) = 104 \pm 18$ (Fig. 4D). From the values of the characteristic times for the exponential variation of AF, we could calculate, as explained above, $PDT_{\text{flask}} = 25 \pm 6 \text{ h}$ and $PDT_{\text{STBR}} = 25 \pm 3 \text{ h}$ (Fig. 4E). Three remarks can be made. First, these PDT values are significantly lower than those derived from 2D cultures, indicating again that the expansion is greatly improved in 3D, as evidenced by the low number of dead cells in capsules (Fig. 4F) compared with 2D colonies (Fig. S6). Second, the AF values are about twice as low as the ones derived from the measurements at the single capsule level. Third, the absence of statistical difference between the two culture systems suggests that, while the impeller-induced shear stress does not affect cell viability, stirred suspension culture in a benchtop bioreactor with expected better homogenization does not enhance the expansion under the experimental conditions selected here.

Additionally, we performed flow cytometry analysis and found that more than 92% of the cells were positive for SOX2, NANOG or OCT4. Stemness thus remains high and similar between static and stirred cultures (Fig. S7), indicating that, by contrast with previous reports [34], shear stress does not trigger the differentiation of hiPSC colonies grown in hollow capsules. Finally, to confirm that the amplification factors reported above are not hiPSC line specific, we carried out the same series of experiments for the other three cell lines in static culture (Fig. 4E). Not only are the differences between cell lines not significant, but their

PDT in 3D is also found very close to the value derived for the commercial hiPSC line that we have extensively investigated in this section, i.e. $PDT_{\text{flask}} = 27 \pm 2 \text{ h}$ by averaging over all three cell lines.

Capsule size and oxygen tension are two parameters that allow to increase hiPSCs fold expansion.

As shown above, the static or stirred batch cultures of hiPSC colonies in capsules yielded amplification at day 7 about twice as low as the one measured at the single capsule level. Although this difference only corresponds to a 3 h difference in PDT, we sought to address this issue and find out solutions to further improve the amplification of hiPSC in batch for large-scale production. We investigated the impact of two possible parameters.

First, we tested whether hiPSC amplification depends on the cell seeding density. The most obvious way would be to increase the volume fraction of cells in the core solution loaded to the microfluidic injector. However, this would lead to earlier and more frequent harvesting. Instead, we pursued a different strategy. We kept the cell density constant but increased the size of the capsules by changing the nozzle diameter [25]. Doing so, for a given volume of the encapsulation cell suspension, the number of produced capsules is indeed reduced by $(R_{\text{big}}/R_{\text{small}})^3$, but the mean number of cells per capsule, λ , is increased by the same fold. In the context of sparse distribution, Poisson statistics applies, and the generation of 300 μm in radius capsules instead of 200 μm leads to an increase in λ by about 3-fold. The immediate consequence is that the probability of obtaining capsules containing no cells is decreased from about 8% to negligible ($\sim 0.03\%$). But, more

importantly, the probability of getting capsules with only one cell, which may die or exhibit some lag phase before proliferation, goes from 20% to 0.3%. A high occurrence of capsules loaded with only one cell is expected to lower the effective amplification factor and thus to increase the doubling time of the cell population. Fig. 5A shows representative phase contrast images of 300 μm in radius capsules filled with hPSC colonies. Noteworthy, most capsules contain several cysts, suggesting that cyst growth was nucleated from several cell aggregates. More quantitatively, after monitoring the growth kinetics in benchtop STBR ($N = 2$), derivation of the time constant reveals shorter doubling time in big capsules: $\text{PDT}_{\text{big}} = 22 \pm 1 \text{ h} < \text{PDT}_{\text{small}} = 25 \pm 1 \text{ h}$ (Fig. 5B).

Second, we pursued our physiomimetic approach. Among all factors that constitute a stem cell niche, we have already pointed out interactions with the ECM. However, until now, we have omitted to consider oxygen tension, which is known to be naturally low in developing embryos [35]. This low level of oxygen was further shown to be key to reduce mutation rates and epigenetic alterations [36,37] as well as to improve the expansion rate [38] while reducing the probability of unwanted differentiation [39]. We thus performed the same culture experiments in big capsules (300 μm radius) by decreasing the dissolved oxygen level (DO) from 100% to 20%. (see Methods section). Under these hypoxic conditions, the population doubling time derived from the growth kinetics was found to be $\text{PDT}_{\text{big}}^{\text{hypoxia}} = 20.4 \text{ h}$ (Fig. 5B), i. e., slightly but significantly shorter than in normoxic conditions. Remarkably, this value is better than the one found at the single capsule level in normoxia, suggesting that the optimization of capsule size and oxygen tension allowed to upscale the production of hPSCs in a bench-scale bioreactor without any degradation of the expansion efficiency.

To assess whether this protocol is not only theoretically scalable but can be genuinely upscaled to an industrial level, we carried out a final experiment in duplicate in a 10 L STBR (Fig. 5C, S8 and Movie S5) by keeping all other parameters constant. Fig. 5D shows the expansion-fold as a function of time. The two curves from these two independent experiments are superimposable, and we found $\text{AF}_{10\text{L STBR}}(6.5 \text{ days}) = 277 \pm 5$, corresponding to a doubling time $\text{PDT}_{10\text{L STBR}} = 19.6 \text{ h}$.

Supplementary data related to this article can be found at <https://doi.org/10.1016/j.biomaterials.2023.122033>.

These data were obtained without passaging. To assess the robustness of the approach for a seed train of passaging and demonstrate that the technology can be integrated into a classical cell therapy production, we performed serial passaging. At harvest after about seven days, the capsules were dissolved, the 3D colonies were dissociated, and cells re-encapsulated following the same protocol (Fig. 6). We found that expansion-fold and stemness were preserved over two consecutive encapsulations within 14 days (Fig. S9).

3. Discussion

In this work, we have developed an *in vitro* culture system for hiPSCs that combines the benefits of biomimetic 3D culture and scalable bioreactor-based production (Fig. 6). By contrast with other approaches using scaffold embedding in a bulk matrix [40] or hydrogel beads [41, 42], our hollow capsules allow provide handleable ECM-laden compartments favorable for hiPSC proliferation and self-organization into 3D colonies that are morphologically reminiscent of epiblasts [43]. While cell-cell interactions are not impaired due to the absence of unwrapping scaffold, the presence of the shell also provides mechanical protection against impeller damage and turbulence-induced so-called Kolmogorov eddies during stirring [44]. Besides exploiting both the biomimetic and protective properties of the developed platform, we have finally refined the culture conditions by tuning the initial mean number of cells per capsule and the oxygen tension. A combination of all these critical factors allowed us to upscale the production of hPSCs and demonstrate that the expansion yield is scale-independent. We could reach 277-fold expansion in 6.5 days in a 10 L stirred-tank bioreactor. To

the best of our knowledge, this expansion efficiency and scalability levels are unmatched in the field [2,45–47]. Other groups indeed managed to handle large-volume cultures in industrial bioreactors but with lower amplification rates [48] or achieved ultra-high cell densities in small bioreactor volumes and with moderate expansion (70-fold expansion in 7 days in 150 mL bioreactors with a final density of 35×10^6 cells/mL) [17]. To ensure a rigorous comparison between the approaches, we must acknowledge that cell density is significantly lower with our technology, of the order of 2×10^6 cells/mL. This is a direct consequence of the presence of lumen that can be seen as lacunae in the hiPSC colonies. Since filling (or collapse) of the lumen beyond confluence was not observed to impair stemness (Fig. S2), there are possibilities to increase the harvesting cell density by simply prolonging the culture by 1–2 days if necessary. Whether preserving the biomimetic cyst morphology of hiPSC colonies in the perspective of manufacturing high-quality hiPSC is more important than increasing the cell density, however, remains to be investigated in depth.

Beyond collecting these numbers that characterize the performances of hPSC bioprocessing strategies, it is important to keep in mind which underlying parameters are truly critical. Since the amplification factor $\text{AF}(t)$ of a culture system is given by $\text{AF}(t) = 2^{t/\text{PDT}}$, where PDT accounts both for cell division and cell death, we may rewrite it as $\text{AF}(t) = 2^{(k_+ - k_-)t}$, where k_+ and k_- are respectively the division and death rate of cells. Thus, the upper theoretical limit for AF is obtained for $k_- = 0$ (i.e. infinite death time), which then yields a minimal PDT_{min} value, equal to k_+ . Even though precise measurements of k_+ , or equivalently, the duration of the cell cycle $t_+ = 1/k_+$ of hPSC are scarce in the literature, the cell cycle duration in human and mammalian ESC was reported to be $t_+ = 11\text{--}16\text{-h}$ [49,50], and more recently the one of primed pluripotent in 2D culture was found to be $t_+ \sim 14 \text{ h}$ [51]. By assuming that the duration of the cell cycle in the 3D cyst topology is identical to the value obtained in 2D cultures, with $\text{AF}(t = 6.5 \text{ days}) = 277$ corresponding to $\text{PDT} = 19 \text{ h}$, we find that the PDT of the encapsulated hiPSC colonies is only $5 \pm 2 \text{ h}$ longer than the intrinsic cell cycle duration. The difference between PDT and t_+ corresponds to a death rate $k_- = 1/53 \text{ h}^{-1}$. By comparison, in the seminal Yamanaka's paper [23], doubling times in 2D hiPSC colonies of about 45 h give $k_- = 1/20 \text{ h}^{-1}$. More meaningful than the death rate k_- , the fraction of dead cells can be roughly estimated as $\varphi_{\text{dead}} \approx \frac{2^{k_+ t} - 1}{2^{k_+ t}} = 2.6\%$ at $t = 6.5$ days, while cell counting gives 1.30% in bioreactors and 1.97% in flasks (Fig. S6). In 2D cultures, we measured a fraction of dead cells of the order of 12% at harvest, even though this value under-estimates the cumulated mortality which is drastically impacted by cell passaging [52]. Further expansion improvement is theoretically within reach by vanishing the cell death rate. Taking again $t_+ \sim 14 \text{ h}$ for the cell cycle length of hiPSC, the glass ceiling is calculated to be $\text{AF}_{\text{max}}(t = 6.5 \text{ d}) \sim 2200$. However, the value of $t_+ \sim 14 \text{ h}$ cannot be taken as granted and a significant cell density-dependence on t_+ cannot be discarded. Indeed, hPSC were shown to exhibit a decelerated proliferation due to a prolonged G1 phase as cell density increases [53]. Similarly, smaller expansion rates were observed when the inoculation density either as single cells or pre-clusters in a synthetic hydrogel exceeds 10^6 cells/mL [40]. We may then anticipate that the actual average cell cycle duration could be longer than the one reported above upon single-cell lineage tracking in small colonies of hPSCs. As a consequence, even though future work should aim at a rigorous *in situ* measurement of the division rate within the encapsulated hiPSC cysts, we cannot exclude that the unprecedented hiPSC expansion rates reported in this work are approaching the glass ceiling.

Among other advantages of the proposed technology, we mentioned the protective role of the alginate shell and the scale-independence of the culture conditions. By contrast with other suspension cultures that need to design specific low-shear impellers (e.g. the vertical-wheel bioreactor [54,55], or to add shear-dampener polymers (e.g. pluronics [17]) to avoid stirring-induced cell damages, our capsules permit the use of standard industrial scale bioreactors.

However, all the benefits cannot be assigned to this sole shielding effect. Indeed, previous works had already proposed to embed either hESC aggregates or microcarriers within hydrogel beads (referred to as capsules in these original works) [42] to improve cell viability. Nonetheless, fold expansion rates were not reported to be larger than 10 in 19 days. Similarly, two recent works describe stem cells' encapsulation in hollow capsules [56,57]. However, the absence of ECM leads to the formation of aggregates and a modest amplification (estimated to be 70-fold in 8 days from the size of the encapsulated spheroids). We thus propose that the significant amplification increase obtained here mainly originates from the ECM-based stem cell environment engineered within each capsule, which drives hiPSC multicellular organization into cysts. In the present work, Matrigel was used as an ECM gel inside the capsules. Matrigel contains multiple growth factors and is known as a potent *in vitro* inducer of cell growth, thus expected to rescue dying cells and promote cell proliferation. In a previous work [26], we demonstrated that co-encapsulation of cells and Matrigel leads to a continuous, homogeneous, and anchored coating of the capsules' inner walls provided that Matrigel's volume fraction is at least 25%. This localized cross-linking of Matrigel was proposed to be related to the chemical affinity between laminin (one of the main components of Matrigel) and sodium alginate. We hypothesize that this interpenetrating coating could provide a substrate that offers biochemical and biomechanical cues for nascent clumps of hiPSC to grow into cysts. We are however aware that Matrigel, as a mouse tumor ECM mixture, has limitations for further use in regenerative medicine due to its mouse and tumor-derived origin. Even though it is still widely used for lack of better, novel synthetic or natural scaffolds are explored [58,59] and could advantageously serve as alternatives to Matrigel in the encapsulation process described in the present work.

Interestingly, numerous studies have recently proposed biomimetic controllable environments that can be used to develop PSC-based embryo models and, more specifically epiblast models [13,60]. In all cases, these so-called stem cell niche-like environments drive PSCs self-organization, luminogenesis, and polarization into pseudo-stratified epithelia [8–10]. This cyst configuration, which seems to be key in developmental processes, may be regarded as an optimized configuration for hPSC expansion with minimal loss of viability [61]. First, it is well accepted that 2D hiPSC cultures exhibit intra-colony heterogeneities in pluripotency marker genes [62], viability [63] and cell morphology [64], which are very striking between the center and the edges of the colonies. In this respect, the closed spherical symmetry of a cyst intrinsically suppresses the “center-edge phenotype” and may result in a more homogeneous cell population [65]. Additionally, whereas cellular crowding or compaction are known to inhibit proliferation or even trigger apoptosis via caspase-dependent mechanisms [66], a cyst configuration is less prone to stress building in bulk due to the presence of a lumen. Similarly, a fast proliferation rate may contribute to stress relaxation and reduce cell extrusion occurrence, as observed in epithelia under compression [67,68]. Besides mechanical stress, chemical stresses increase the mutation rate [36,69]. Using bioreactors with precise adjustment of physioxia, pH, lactate, glucose and nutrients supply is thus instrumental and could be optimized beyond the present achievement.

Finally, relying on the observation that chromosome segregation fidelity is unambiguously higher in native contexts of epithelia of primary cells [70,71], it also becomes tempting to speculate that, beyond the gain in amplification it provides, the preserved histology of our 3D hiPSC colonies could also be beneficial to the maintenance of the genetic integrity [72].

In summary, our work has shown that hollow alginate capsules with reconstituted niche-like microenvironment can promote the formation and growth of 3D hPSC colonies and provide the necessary protection for scaling up the production in stirred tank bioreactors. Self-organized encapsulated colonies seem to be instrumental for optimal expansion by preserving stem cells physiological properties. We have demonstrated

that our stem cell technology can deliver unprecedented scalability. We anticipate that cell quality is maintained on the basis of extremely high viability, which is taken as a primary signature of cell fitness. Future works should focus on assessing the hPSCs quality in *in vivo*-like culture systems since the emergence of mutations during culture may be the last limitation to overcome for cell therapy bioproduction.

4. Online Methods

4.1. Ethics statements

The generation, use and storage of hiPSCs were performed with approval from the “Comité de Protection des Personnes” (CPP) Ile de France (DC 2015–2595 and 2016-A00773-48).

4.2. Human pluripotent stem cell lines

Throughout the present work, we used 4 hiPSC lines. Among these, 3 hiPS cells, namely IMAGINi004-A (referred to as iPS 004), IMAGINi005-A (iPS 005) and IMAGINi013-A (iPS013) were derived from peripheral blood mononuclear cells (PBMC) according to the protocol described in Ref. [73]. Briefly, PBMCs were transduced using the CytoTune-iPS 2.0 Sendai Reprogramming Kit (ThermoFisher Scientific) following the manufacturer's instructions. After 2–3 weeks, colonies were manually picked and expanded at least 10 passages. The 4th hiPSC line is a commercial line from ThermoFisher: Gibco™ episomal hiPSC line (A18945) generated using cord blood derived CD34⁺ progenitors with 7 episomally expressed factors (Oct4, Sox2, Klf4, Myc, Nanog, Lin 28, and SV40 T). This commercial cell line is referred to as iPS C. For the sake of availability, to allow other groups to reproduce our findings, all experiments reported here were performed with iPS C, except for those that are described in Figs. 2F, 3A and 3B, 3D, 4E and Figures S4 and S5, which were carried out to demonstrate that the findings were not cell line-dependent.

4.2.1. 2D hiPSC culture

All hiPSC lines were maintained on Matrigel (Corning Ref. 354,234) and cultured in mTeSR1 medium (StemCell Technologies 85,875). Cultures were fed daily, passaged with an enzyme-free reagent, ReLeSR (StemCell Technologies 05873) at 0,11 mL/cm² for 5 min at 37 °C. every 3–6 days (around 80% confluency), and replated as small clusters (between 100 and 200 μm) at a density of about 5000–10000 cells/cm². Cells were cultured at 37 °C in a humidified atmosphere containing 5% CO₂. The last 2D cell culture passage (before encapsulation) was done using accutase (StemCell ref. 07920) at 0.08 mL/cm² for 8 min at 37 °C.

4.3. 3D hiPSC encapsulation

Before encapsulation, 2D stem cell colonies were detached using ReLeSR for 1 min and dissociated into a near single-cell solution using Accutase (Stem Cell Technologies 07920). HiPSCs were then mixed in a 50/50 vol ratio with Matrigel at 4 °C to keep the suspension in a liquid state. The final concentration of cells in the cell/matrix solution was thus between 0.4 and 1.0 × 10⁶ viable cells/mL, referred to as the encapsulation density. The encapsulation system is similar to the one described in Ref. [26]. In brief, ethylene tetrafluoroethylene (ETFE) tubings are connected to the three inlets of a 3D printed (using the DLP Micro Plus Hi-Res printer from EnvisionTEC) microfluidic co-laminar flow device. An extruded and polished glass microcapillary tip (of diameter ~100 μm for most experiments reported in this work, at the exception of those shown in Fig. 5A–B that were carried out with a nozzle diameter of 150 μm) is glued to the outlet of the nozzle for a better control of the flow. The cell/matrix suspension is loaded into the inner channel of the 3-way device, which is kept refrigerated thanks to an in-line cooling system in order to prevent premature gelation of Matrigel. A solution of sodium alginate (Novamatrix Pronova SLG100, 0.25 g #4202101 at 2% in

distilled water) is injected into the outer channel. To prevent alginate gelation within the microfluidic device due to calcium release from the suspended cells, a calcium-free solution (Sorbitol 300 mM, Sigma-Aldrich 85,529) is used in the intermediate channel of the co-extrusion chip and serves as a barrier against calcium diffusion. Typical flow rates for the 3 solutions were on the order of 120 mL/h for all three channels: (the alginate solution, the sorbitol solution and the cell + matrix suspension). At these rates, the composite solution forms a liquid jet that fragments into droplets (of about twice the size of the nozzle) due to the spontaneous Rayleigh-Plateau instability. To avoid subsequent coalescence of the train of droplet, an alginate charging part and a copper ring are connected to a high voltage (2000V) generator are introduced. A high-speed camera (PHANTOM VEO 1310 L) was used to visualize droplet formation and splay (Fig. S1 and Movie S1). When the composite droplets contact the collecting calcium bath (at 100 mM), the outer layer of alginate readily gels. As a consequence, the inner cell/matrix solution remains entrapped inside a closed, spherical and permeable micro-compartment. Within 1 min following encapsulation, capsules are rinsed with medium (DMEM) to reduce the basal calcium concentration. Finally, they are transferred to a suspension culture medium.

Re-encapsulation was performed by the dissolution of alginate shells using a short ReLeSR rinse, followed by cell dissociation using TrypLE (Trypsin-based, dissociation enzyme, ThermoFisher) for 20 min at 37 °C. Then the obtained cells were processed following the classic encapsulation protocol.

4.4. 3D stem cell suspension culture in static T-flasks or bioreactors

Static suspension cultures of encapsulated hiPSC were carried out using T-flasks (from 5 to 30 mL) maintained in a cell culture incubator at

37 °C and 5% CO₂. The medium (mTeSR1) was supplemented with 10 μM Y-27632 for ROCK inhibition only during the first 24 h of culture. From culture day 3, the medium was exchanged every day as described hereafter. The contents of the T-flasks were transferred into Falcon Tubes. After capsules sedimentation (within a few minutes), the supernatant was removed and replenished as the capsules were transferred back into a T-flasks. The volume of culture medium was kept constant for the first 4 days of culture (~4 × the capsules volume). Then, the volume was steadily increased every day in order to maintain a cell concentration below 10⁶ cells/mL.

Stirred suspension cultures were performed in different bioreactors. For all experiments reported in Figs. 4 and 5A-B, we used benchtop STBRs, including a 30 mL (Minibio, ABLE® Bioreactor Systems) or 500 mL bioreactors (Applikon Biotechnology & Global Process Concept). For the experiments reported in Fig. 5C–D, we used a 10 L-scale bioreactor (Global Process Concept). In this latter case, in order to reduce the encapsulation time, hiPSC capsules were generated using 4 setups working in parallel. The stirring speeds were set at 150 rpm, 80 rpm, 40 rpm in 10 L, 500 mL and 30 mL STBRs respectively.

In all cases, the bioreactors were inoculated with 15% capsule-to-medium volume. The bioreactor culture starts at a volume representing 30% of the final working volume. At the day 1, the medium was replaced with fresh medium without ROCK inhibitor. From day 2–5, the culture is performed in a fed-batch mode up to the final working volume (22). Then, we switched to repeated-batch mode, where 90% of the media was daily renewed to maintain sufficient nutrient supply. The final capsule-to-medium volume was 4.2 ± 0.3% and the pH was maintained at 7.2 ± 0.2.

Dissolved Oxygen (DO) level is calibrated at 100% in starting conditions by injecting air into the bioreactor headspace. During the run, the oxygen level is monitored and controlled. In normoxic conditions,

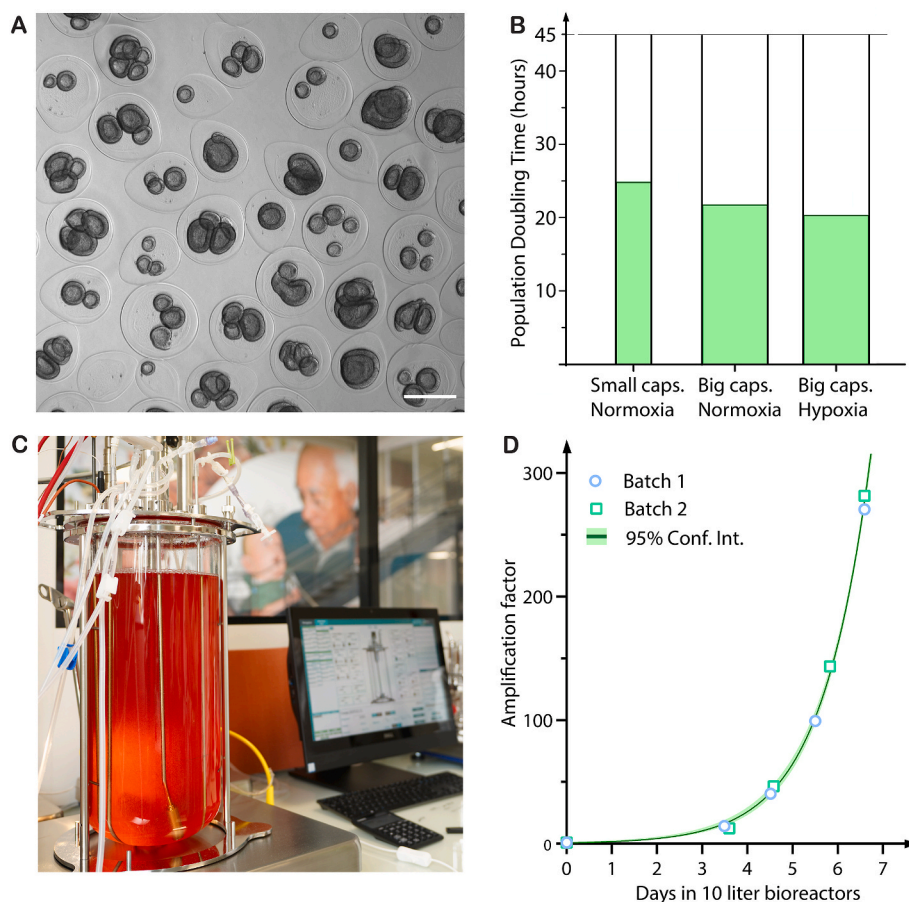


Fig. 5. Impact of capsule size and oxygen tension on hPSC amplification and scalability in stirred tank bioreactors (A) Phase contrast image showing 3D hiPSC colonies in capsules referred to as “big” in the main text (with an average radius of 300 μm). Scale bar = 500 μm. (B) Population doubling time of encapsulated 3D hiPSC colonies cultivated in benchtop bioreactors by varying the size of the capsules and the oxygen tension conditions (normoxic versus hypoxic). (C) Picture of a 10 L industrial stirred tank bioreactor used to test the scalability of the stem cell capsule culture system. (D) Graph of amplification factor of hiPSCs grown in 10 L bioreactors over a week, in ‘Big capsules’ and hypoxic conditions; Data were obtained from 2 independent batches and from 2 independent encapsulations. Light green band shows the 95% confidence interval of the fitting curve. (For interpretation of the references to colour in this figure legend, the reader is referred to the Web version of this article.)

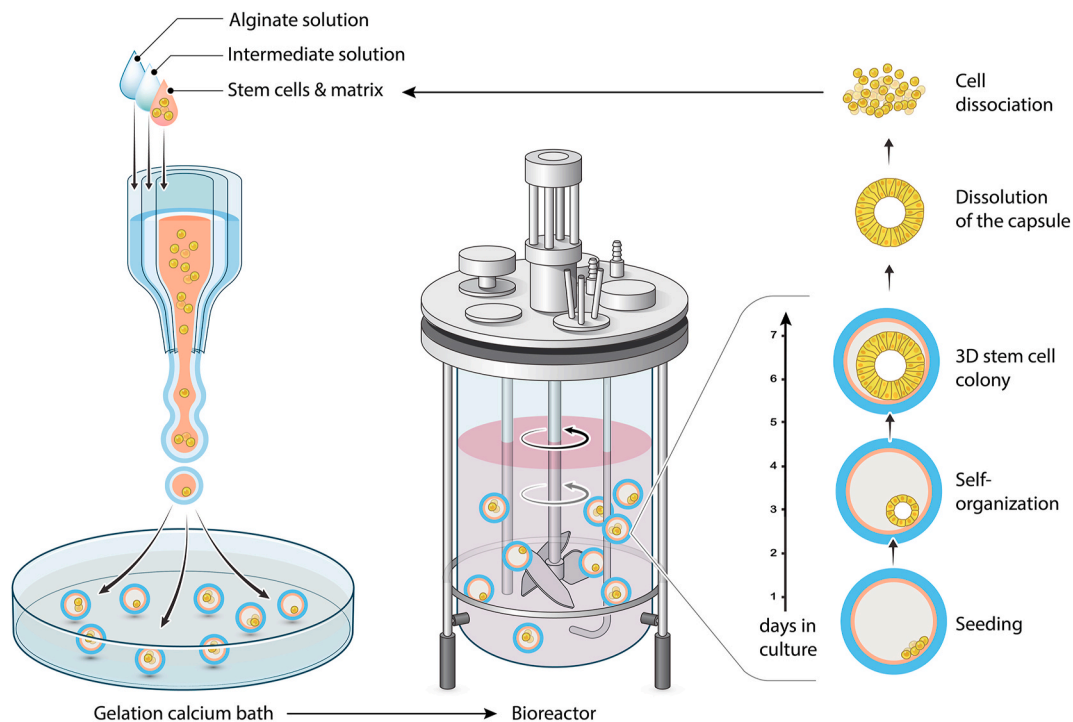


Fig. 6. Encapsulation and scale-independent culture of encapsulated 3D hPSC colonies in bioreactors. After encapsulation using the microfluidic extrusion technique (left panel), hPSC in matrix-laden capsules are transferred to suspension culture in a bioreactor (middle panel). Under controlled conditions provided by the bioreactor, hPSC cells self-organize into cysts which are protected by the capsules. These growing 3D colonies are harvested and dissociated after capsule dissolution. Subsequent cell suspension may then serve for another encapsulation and expansion.

the oxygen is controlled at 100% while in hypoxic conditions the set point is at 20% DO. Oxygen level is regulated by sparging nitrogen and/or air to maintain the set point. 10 L scale bioreactors were regulated in hypoxic conditions.

4.4.1. Time-lapse microscopy of encapsulated cyst growth and image analysis

Time-lapse microscopy was performed using a Nikon Biostation IM microscope with a 10x objective. Capsules containing hiPSCs were transferred to a 35 mm Petri dish 24 h after encapsulation. Approximately 10–20 capsules were placed in the Petri dish containing 5 mL of fresh Y-27632-free mTeSR1 medium. Cyst growth was monitored over 7 days. Practically, images were taken every 6–10 min at preselected Z-focal planes to ensure acquisition at proper focus in case of undesired drift. Image analysis was performed using ImageJ built-in routines to detect particle contours and analyze the morphology. The external and internal effective radii of the cysts, R_{out} and R_{in} , were measured from the equatorial corresponding cross sections S according to $R_{out,in} = (S_{out,in}/\pi)^{1/2}$ after applying appropriate bandpass filters and thresholds. The volume V of the cells was calculated as $V = 4\pi/3 (R_{out}^3 - R_{in}^3)$. Capsule circularity was defined as $C = a^2/b^2$, where a and b are the short and long axes of the approximated ellipse.

4.4.2. In vitro trilineage differentiation

2D hiPSCs were manually cut into small cell clumps under a stereomicroscope following a standard protocol [59]. 3D, hiPSC colonies were decapsulated and dissociated (see protocols above). Clumps collected from 2D or 3D culture were transferred into ultra-low attachment dishes (Corning, Ultra-low attachment 6 well plate). 3D aggregates of cells composed of an amalgam of the three developmental germ layers (embryoid bodies (EBs) [74]) formed spontaneously and were cultured in suspension for 7–9 days with DMEM/F-12 medium containing 20% pluriQ Serum Replacement (GlobalStem), 1% non-essential amino acids, 1% penicillin-streptomycin and 0.2%

β -mercaptoethanol (ThermoFisher Scientific) in a humidified atmosphere containing 5% CO_2 . Culture medium was refreshed every two days. EBs were then collected for RNA analyses or transferred onto gelatin-coated dishes for 1 week. For immunocytochemistry analysis, cells were fixed with 4% paraformaldehyde for 15 min at room temperature (RT). After washing in PBS/1%BSA blocking solution for 1 h, cells were incubated overnight at 4 °C with primary antibodies, washed 3 times in PBS, and incubated with secondary antibodies for 2 h at RT. Antibodies were diluted in PBS/1%BSA/0.1%Triton solution. The list of antibodies used in this work and their origin are listed in Table S1. Nuclei were stained with a DAPI solution. Immuno-fluorescence staining was analyzed using the Celena S™ Digital Imaging System (Logos Biosystems).

4.5. RNA extraction and RT-PCR analyses

Total RNA was extracted using the RNeasy Mini Kit (Qiagen). cDNA was synthesized using a high capacity cDNA RT kit (ThermoFisher Scientific) from 1 μ g of total RNA. The expression of pluripotency markers as well as the trilineage differentiation potential of the cells were evaluated by TaqMan® hiPSC Scorecard™ assay according to the manufacturer's protocol. This scorecard compares the gene expression pattern of key pluripotency and germ lineage markers relative to a reference standard that consists of 9 different human ES and iPS lines [75,76]. Data analysis was performed using the cloud based TaqMan® hiPSC Scorecard™ analysis software.

4.6. DNA isolation, genomic stability and authenticity analysis

DNA isolation was performed using the PureLink™ Genomic DNA Mini Kit (Invitrogen). Molecular karyotype was performed using an Infinium Core-24 v1.2 Kit (Illumina) containing 300,000 SNPs. Data were analyzed with BeadStudio/GenomeStudio software (Illumina). The log R ratio shows the intensity signals of the SNPs, which indicates gains

or losses. The B allele frequency gives information about the genotype as a measure of allelic ratio. For each SNP, comparisons of the genotype before and after cell encapsulation have been performed. The percentage of SNP concordance between iPSC samples before and 7 days after encapsulation was assessed for the 3 derived iPSC cell lines. SNP files of all samples were extracted from genome studio software. The percentage of concordance between two paired samples (before and after encapsulation) was evaluated by comparing the genotype of each informative SNP (Fig. S5).

4.6.1. Flow cytometry analysis

The hiPSCs colonies were dissociated with Accutase for 10 min at 37 °C for 2D cultures or with TrypLE Select (ThermoFisher Scientific 11,598,846) for 30 min at 37 °C for 3D cultures after capsule removal. Then, cells were fixed and permeabilized using the Transcription Factor Staining Buffer Set (ThermoFisher 11,500,597). Cells were suspended in the permeabilization buffer at a density of $0.5\text{--}1 \times 10^6$ cells in 100 μL and incubated with the specific antibodies or isotype controls (Table S1) for 45 min at room temperature in the dark. Cells were washed twice with the staining buffer and analyzed using either BD Canto II (at the TBMCore CNRS UMS 3427 – INSERM US 005) or a BD Accuri™ C6 plus. Isotype controls were performed to determine the limit of positivity above which a sample will be considered positive. The threshold of positivity is when less than 3% of cells labeled with the control isotype are positive. Samples were reported positive if they were above the positive threshold. Compensation controls for each fluorochrome were used to set up cytometer alignment and to remove spectral overlap. and d Data was post-processed with FlowJo software. Gating was performed on the basis of isotype negative control to differentiate stemness-specific antibody staining and non-specific background signal. Significant signal of both NANOG+ and OCT4+ population is therefore used to identify and calculate the percentage of pluripotent cells in the sample.

4.6.2. Cell growth and viability analysis

Cell counting was performed using the Nucleo counter NC3000 or NC200 (Chemometec). Live/dead analysis was performed using CalceinAM/Ethidium homodimer-1 (ThermoFisher L3224) according to the manufacturer recommendations, and samples were imaged using either the EVOS FL or EVOS M5000 auto Imaging system (ThermoFischer).

4.7. Immunostaining, microscopy, and image analysis

For daily brightfield imaging of 2D cultures and encapsulated hiPSC cysts, a widefield EVOS FL or EVOS M5000 automated microscope was used. Encapsulated 3D hiPSC colonies were harvested for confocal microscopy at several timepoints. The alginate capsule was removed prior to fixation by incubating the samples in a short rinse of ReLeSR at RT, which serves here as a calcium chelator that gently dissolves the alginate gel. Both 2D and 3D stem cell colonies were fixed with 4% PFA for 30–60 min at RT in the dark. Following fixation, the samples were washed 3x with 0.1% Tween20 in PBS. A permeabilization step was done in parallel with excess PFA quenching in a PBS solution containing 0.3% Triton X-100 and 100 mM glycine for 30 min, followed by 3x washing with 0.1% Tween20 in PBS. The samples were incubated in primary and secondary antibodies (Table S1) in 1% BSA + 0.1% Tween20 in PBS overnight at 4 °C with gentle orbital agitation, including a 3x rinsing with 1% BSA + 0.1% Tween20 in PBS after each incubation. To maintain alginate capsules during fixation and staining, the decapsulation step was skipped and all solutions (including 4% PFA) were supplemented with calcium and magnesium. All samples were imaged on either a Leica SP5 or SP8 confocal microscope (Bordeaux Imaging Center, BIC).

4.8. Statistical analysis

All statistical analyses were performed using GraphPad Prism 8. The

differences between bioreactor and flask culture performances could not be tested due to insufficient sampling. Graphs and regression lines thus have only an indicative purpose. In the other cases described, Student T-test was used. All statistical significance is reported in terms of p-values <0.05.

Credit author statement

KA, NL and MF designed the project and supervised experiments and analysis; PC performed the experiments, analyzed the data and wrote the article; Experiments were performed both at the Imagine Institute and at Treefrog Therapeutics (TFT). AL helped to perform experiments, analyzing the data and writing the article; EL, FM and ML designed bioreactor cultures and scale-up, EL, JP, HW, EJ and MD performed bioreactor cultures; JC EW EQ CB EP contributed to 2D cultures, encapsulations, trilineage assay and SNP analysis; BG contributed to data analysis and writing.; PVL proposed a mathematical formulation for PDT and viability. PN helped analyze the growth of 3D colonies and write the manuscript. KA, CR and JH conceived and produced the microfluidic chips and performed high-speed camera recordings.

Funding

This work was supported in part by funding grants from European commission H2020-EIC-SMEInst (grant agreement number: 881,113 C-stemGMP), iLAB2018 Bpi France, Region Nouvelle Aquitaine and Agence Nationale pour la Recherche (ANR-17-C18-0026-02). We acknowledge the Bordeaux Imaging Center, a service unit of the CNRS-INSERM and Bordeaux University, member of the national infrastructure France BioImaging supported by the French Research Agency (ANR-10-INBS-04). We acknowledge the TBMCore facility. (CNRS UMS 3427 – INSERM US 005). We also thank Nicolas Doulet and Marion Pilorge for helping build the collaboration between Treefrog Therapeutics and the Imagine Institute.

Declaration of competing interest

The authors declare the following financial interests/personal relationships which may be considered as potential competing interests: Feyeux has patent #WO2018096277A1 issued to assignee. Nassoy has patent #WO2018096277A1 issued to assignee. Alessandri has patent #WO2018096277A1 issued to assignee. MF and KA are the founders of TFT; MF, KA, PC and PN are shareholders of Treefrog Therapeutics. MF, KA and PN have a patent pertaining to discoveries presented in this manuscript. Patent no: WO2018096277A1.

Data availability

Data will be made available on request.

Acknowledgments

Appendix ASupplementary data

Supplementary data to this article can be found online at <https://doi.org/10.1016/j.biomaterials.2023.122033>.

References

- [1] A.S. Mao, D.J. Mooney, Regenerative medicine, Current therapies and future directions, *Proc. Natl. Acad. Sci. U.S.A.* 112 (2015) 14452–14461, <https://doi.org/10.1073/pnas.1508520112>.
- [2] M.M. Adil, D.v. Schaffer, Expansion of human pluripotent stem cells, *Current Opinion in Chemical Engineering* 15 (2017) 24–35, <https://doi.org/10.1016/j.coche.2016.11.002>.

- [3] J.A. Thomson, Embryonic stem cell lines derived from human blastocysts, *Science* 282 (1998) 1145–1147, <https://doi.org/10.1126/science.282.5391.1145>.
- [4] K. Takahashi, K. Tanabe, M. Ohnuki, M. Narita, T. Ichisaka, K. Tomoda, S. Yamanaka, Induction of pluripotent stem cells from adult human fibroblasts by defined factors, *Cell* 131 (2007) 861–872, <https://doi.org/10.1016/j.cell.2007.11.019>.
- [5] E. Kuijk, M. Jager, B. van der Roest, M. Locati, A. van Hoeck, J. Korzelius, R. Janssen, N. Besselink, S. Boymans, R. van Boxtel, E. Cuppen, Mutational impact of culturing human pluripotent and adult stem cells, *Nat. Commun.* (2018), 430165, <https://doi.org/10.1101/430165>.
- [6] K. Garber, RIKEN suspends first clinical trial involving induced pluripotent stem cells, *Nat. Biotechnol.* 33 (2015) 890–891, <https://doi.org/10.1038/nbt0915-890>.
- [7] S. Yamanaka, Pluripotent stem cell-based cell therapy-promise and challenges, *Cell Stem Cell* 27 (2020) 523–531, <https://doi.org/10.1016/j.stem.2020.09.014>.
- [8] K. Taniguchi, Y. Shao, R.F. Townshend, Y.H. Tsai, C.J. Delong, S.A. Lopez, S. Gayen, A.M. Freddo, D.J. Chue, D.J. Thomas, J.R. Spence, B. Margolis, S. Kalantry, J. Fu, K.S. O'Shea, D.L. Gumucio, Lumen Formation is an intrinsic property of isolated human pluripotent stem cells, *Stem Cell Rep.* 5 (2015) 954–962, <https://doi.org/10.1016/j.stemcr.2015.10.015>.
- [9] M.N. Shahbazi, A. Scialdone, N. Skorupska, A. Weberling, G. Recher, M. Zhu, A. Jedrusik, L.G. Devito, L. Noli, I.C. MacAulay, C. Buecker, Y. Khalaf, D. Ilic, T. Voet, J.C. Marioni, M. Zernicka-Goetz, Pluripotent state transitions coordinate morphogenesis in mouse and human embryos, *Nature* 552 (2017) 239–243, <https://doi.org/10.1038/nature24675>.
- [10] Y. Zheng, X. Xue, Y. Shao, S. Wang, S.N. Esfahani, Z. Li, J.M. Muncie, J.N. Lakins, V.M. Weaver, D.L. Gumucio, J. Fu, Controlled modelling of human epiblast and amnion development using stem cells, *Nature* 573 (2019) 421–425, <https://doi.org/10.1038/s41586-019-1535-2>.
- [11] G. Sheng, Epiblast morphogenesis before gastrulation, *Dev Biol.* 1 401 (1) (2015) 17–24, <https://doi.org/10.1016/j.ydbio.2014.10.003>.
- [12] J. Nichols, A. Smith, Pluripotency in the embryo and in culture, *Cold Spring Harbor Perspect. Biol.* 14 (8) (2012) a008128, <https://doi.org/10.1101/cshperspect.a008128>.
- [13] M.N. Shahbazi, Mechanisms of Human Embryo Development : from Cell Fate to Tissue Shape and Back, Development, Cambridge, 2020, p. 147, <https://doi.org/10.1242/dev.190629>.
- [14] Stephen M. Dang, Sharon Gerech-Nir, Jinny Chen, Itskovitz-Eldor Joseph, W. Peter, Ph.D. Zandstra, Controlled, scalable embryonic stem cell differentiation culture, *Stem Cell.* 22 (3) (2004) 275–282, <https://doi.org/10.1634/stemcells.22-3-275>.
- [15] S.M. Dang, P.W. Zandstra, Scalable production of embryonic stem cell-derived cells, in: C.D. Helgason, C.L. Miller (Eds.), *Basic Cell Culture Protocols. Methods in Molecular Biology™*, vol. 290, Humana Press, 2005, <https://doi.org/10.1385/1-59259-838-2-353>.
- [16] M.A. Kinney, C.Y. Sargent, T.C. McDevitt, The multiparametric effects of hydrodynamic environments on stem cell culture, *Tissue Eng. B Rev.* 17 (2011) 249–262, <https://doi.org/10.1089/ten.teb.2011.0040>.
- [17] F. Manstein, K. Ullmann, C. Kropp, C. Halloin, W. Triebert, A. Franke, C.M. Farr, A. Sahabian, A. Haase, Y. Breitkreuz, M. Peitz, O. Brüstle, S. Kalies, U. Martin, R. Olmer, R. Zweigerdt, High density bioprocessing of human pluripotent stem cells by metabolic control and in silico modeling, *Stem Cells Translational Medicine* (2021) 1–18, <https://doi.org/10.1002/sctm.20-0453>.
- [18] B.S. Borys, T. So, J. Colter, T. Dang, E.L. Roberts, T. Revay, L. Larjani, R. Krawetz, I. Lewis, B. Argiropoulos, D.E. Rancourt, S. Jung, Y. Hashimura, B. Lee, M.S. Kallos, Optimized serial expansion of human induced pluripotent stem cells using low-density inoculation to generate clinically relevant quantities in vertical-wheel bioreactors, *Stem Cells Translational Medicine* 9 (2020) 1036–1052, <https://doi.org/10.1002/sctm.19-0406>.
- [19] Y.Y. Lipsitz, C. Woodford, T. Yin, J.H. Hanna, P.W. Zandstra, Modulating cell state to enhance suspension expansion of human pluripotent stem cells, *Proc. Natl. Acad. Sci. U.S.A.* 115 (25) (2018) 6369–6374, <https://doi.org/10.1073/pnas.1714099115>.
- [20] B. Lee, S. Jung, Y. Hashimura, M. Lee, B.S. Borys, T. Dang, M.S. Kallos, C.A. V. Rodrigues, T.P. Silva, J.M.S. Cabral, Cell culture process scale-up challenges for commercial-scale manufacturing of allogeneic pluripotent stem cell products, *Bioengineering* 9 (3) (2022) 92, <https://doi.org/10.3390/bioengineering9030092>.
- [21] J. Colter, K. Murari, J. Biernaskie, M.S. Kallos, Induced pluripotency in the context of stem cell expansion bioprocess development, optimization, and manufacturing: a roadmap to the clinic, *NPJ Regen Med* 6 (1) (2021) 72, <https://doi.org/10.1038/s41536-021-00183-7>.
- [22] Y. Nie, P. Walsh, D.L. Clarke, J.A. Rowley, T. Fellner, Scalable passaging of adherent human pluripotent stem cells, *PLoS One* 7 (2014), <https://doi.org/10.1371/journal.pone.0088012>.
- [23] M. Ma, A. Chiu, G. Sahay, J.C. Doloff, N. Dholakia, R. Thakrar, J. Cohen, A. Vegas, D. Chen, K.M. Bratlie, T. Dang, R.L. York, J. Hollister-Lock, G.C. Weir, D. G. Anderson, Core-shell hydrogel microcapsules for improved islets encapsulation, *Advanced Healthcare Materials* 2 (2013) 667–672, <https://doi.org/10.1002/adhm.201200341>.
- [24] W. Zhang, S. Zhao, W. Rao, J. Snyder, J.K. Choi, J. Wang, I.A. Khan, N.B. Saleh, P. J. Mohler, J. Yu, T.J. Hund, C. Tang, X. He, A novel core-shell microcapsule for encapsulation and 3D culture of embryonic stem cells, *J. Mater. Chem. B* 1 (2013) 1002–1009, <https://doi.org/10.1039/c2tb00058j>.
- [25] F. Alessandri, B.R. Sarangi, V.V. Gurchenkov, B. Sinha, T.R. Kiebling, L. Feltler, K. Rico, S. Scheuring, C. Lamaze, A. Simon, S. Geraldo, D. Vignjević, H. Doméjean, L. Rolland, A. Funfak, J. Bibette, N. Bremond, P. Nassoy, Cellular capsules as a tool for multicellular spheroid production and for investigating the mechanics of tumor progression in vitro, *Proc. Natl. Acad. Sci. U.S.A.* 110 (2013) 14843–14848, <https://doi.org/10.1073/pnas.1309482110>.
- [26] K. Alessandri, M. Feyeux, B. Gurchenkov, C. Delgado, A. Trushko, K.-H.H. Krause, D. Vignjević, P. Nassoy, A.A. Roux, D. Vignjević, P. Nassoy, A.A. Roux, A 3D printed microfluidic device for production of functionalized hydrogel microcapsules for culture and differentiation of human Neuronal Stem Cells (hNSC), *Lab Chip* 16 (2016) 1593–1604, <https://doi.org/10.1039/C6LC00133E>.
- [27] S. Tomotika, On the instability of a cylindrical thread of a viscous liquid surrounded by another viscous fluid, *Proceedings of the Royal Society of London. Series A - Mathematical and Physical Sciences* 150 (1935) 322–337, <https://doi.org/10.1098/rspa.1935.0104>.
- [28] B.S. Freedman, C.R. Brooks, A.Q. Lam, H. Fu, R. Morizane, V. Agrawal, A.F. Saad, M.K. Li, M.R. Hughes, R. vander Werff, D.T. Peters, J. Lu, A. Baccei, A.M. Siedlecki, M.T. Valerius, K. Musunuru, K.M. McNagny, T.I. Steinman, J. Zhou, P.H. Lerou, J. v. Bonventre, Modelling kidney disease with CRISPR-mutant kidney organoids derived from human pluripotent epiblast spheroids, *Nat. Commun.* 6 (2015) 8715, <https://doi.org/10.1038/ncomms9715>.
- [29] S. Assou, J. Bouckenheimer, J. de Vos, Concise review: assessing the genome integrity of human induced pluripotent stem cells: what quality control metrics? *Stem Cell.* 36 (2018) 814–821, <https://doi.org/10.1002/stem.2797>.
- [30] T.E. Ludwig, M.E. Levenstein, J.M. Jones, W.T. Berggren, E.R. Mitchen, J.L. Franke, L.J. Crandall, C.A. Daigh, K.R. Conard, M.S. Piekarczyk, R.A. Llanas, F.A. Thomson, Derivation of human embryonic stem cells in defined conditions, *Nat. Biotechnol.* 24 (2006) 185–187, <https://doi.org/10.1038/nbt1177>.
- [31] C. Kropp, D. Massai, R. Zweigerdt, Progress and challenges in large-scale expansion of human pluripotent stem cells, *Process Biochem.* 59 (2017) 244–254, <https://doi.org/10.1016/j.procbio.2016.09.032>.
- [32] M.S. Croughan, J.P. Hamel, D.I.C. Wang, Effects of microcarrier concentration in animal cell culture, *Biotechnol. Bioeng.* 32 (1988) 975–982, <https://doi.org/10.1002/bit.260320805>.
- [33] C.J. Hewitt, K. Lee, A.W. Nienow, R.J. Thomas, M. Smith, C.R. Thomas, Expansion of human mesenchymal stem cells on microcarriers, *Biotechnol. Lett.* 33 (2011) 2325–2335, <https://doi.org/10.1007/s10529-011-0695-4>.
- [34] D.E. Kehoe, D. Jing, L.T. Lock, E.S. Tzanakakis, D. Ph. Scalable stirred-suspension bioreactor culture, *Tissue Eng.* 16 (2010) 405–421, <https://doi.org/10.1089/ten.tea.2009.0454>.
- [35] M.C. Simon, B. Keith, The role of oxygen availability in embryonic development and stem cell function, *Nat. Rev. Mol. Cell Biol.* 9 (2008) 285–296, <https://doi.org/10.1038/nrm2354>.
- [36] O. Thompson, F. von Meyenn, Z. Hewitt, J. Alexander, A. Wood, R. Weightman, S. Gregory, F. Krueger, S. Andrews, I. Barbaric, P.J. Gokhale, H.D. Moore, W. Reik, M. Milo, S. Nik-Zainal, K. Yusa, P.W. Andrews, Low rates of mutation in clinical grade human pluripotent stem cells under different culture conditions, *Nat. Commun.* 11 (2020) 1528, <https://doi.org/10.1038/s41467-020-15271-3>.
- [37] K. Okazaki, E. Maltepe, Oxygen, epigenetics and stem cell fate, *Regen. Med.* 1 (2006) 71–83, <https://doi.org/10.2217/17460751.1.1.71>.
- [38] P. Abecasis, T. Aguiar, É. Arnault, R. Costa, P. Gomes-Alves, A. Aspegren, M. Serra, P.M. Alves, Expansion of 3D human induced pluripotent stem cell aggregates in bioreactors: bioprocess intensification and scaling-up approaches, *J. Biotechnol.* 246 (2017) 81–93, <https://doi.org/10.1016/j.jbiotec.2017.01.004>.
- [39] T. Ezashi, P. Das, R.M. Roberts, Low O₂ tensions and the prevention of differentiation of HES cells, *Nat. Methods* 2 (2005) 325, <https://doi.org/10.1038/nmeth0505-325>.
- [40] Y. Lei, D.v. Schaffer, A fully defined and scalable 3D culture system for human pluripotent stem cell expansion and differentiation, *Proc. Natl. Acad. Sci. U.S.A.* 110 (2013) E5039–E5048, <https://doi.org/10.1073/pnas.1309408110>.
- [41] S. Swioklo, P. Ding, A.W. Pacey, C.J. Connon, Process parameters for the high-scale production of alginate-encapsulated stem cells for storage and distribution throughout the cell therapy supply chain, *Process Biochem.* 59 (2017) 289–296, <https://doi.org/10.1016/j.procbio.2016.06.005>.
- [42] M. Serra, C. Correia, R. Malpique, C. Brito, J. Jensen, P. Bjoerquist, M.J.T. Carrondo, P.M. Alves, M. Serra, C. Correia, R. Malpique, C. Brito, J. Jensen, P. Bjoerquist, M.J. T. Carrondo, P.M. Alves, Microencapsulation technology: a powerful tool for integrating expansion and cryopreservation of human embryonic stem cells, *PLoS One* 6 (2011) 1–13, <https://doi.org/10.1371/journal.pone.0023212>.
- [43] M.N. Shahbazi, M. Zernicka-Goetz, Deconstructing and reconstructing the mouse and human early embryo, *Nat. Cell Biol.* 20 (2018) 878–887, <https://doi.org/10.1038/s41556-018-0144-x>.
- [44] K. Ponnuru, J. Wu, P. Ashok, E.S. Tzanakakis, E.P. Furlani, Analysis of stem cell culture performance in a microcarrier bioreactor system. Technical Proceedings of the 2014 NSTI Nanotechnology Conference and Expo, NSTI-Nanotech 2 (2014) 132–135.
- [45] A. Polanco, B. Kuang, S. Yoon, Bioprocess Technologies that preserve the quality of iPSCs, *Trends Biotechnol.* xx (2020) 1–13, <https://doi.org/10.1016/j.tibtech.2020.03.006>.
- [46] C.C. Miranda, M.L. Akenhead, T.P. Silva, M.A. Derr, M.C. Vemuri, J.M.S. Cabral, T. G. Fernandes, A dynamic 3D aggregate-based system for the successful expansion and neural induction of human pluripotent stem cells, *Front. Cell. Neurosci.* 16 (2022), 838217, <https://doi.org/10.3389/fncel.2022.838217>.
- [47] C.K. Kwok, I. Sébastien, K. Hariharan, I. Meiser, J. Wihan, S. Altmaier, I. Karnatz, D. Bauer, B. Fischer, A. Feile, A. Cabrera-Socorro, M. Rasmussen, B. Holst, J. C. Neubauer, C. Clausen, C. Verfaillie, A. Ebner, M. Hansson, R. Steeg, H. Zimmermann, Scalable expansion of iPSC and their derivatives across multiple lineages, *Reprod. Toxicol.* 112 (2022) 23–35, <https://doi.org/10.1016/j.reprotox.2022.05.007>.

- [48] Shuohao Huang, Azher Razvi, Zoe Anderson-Jenkins, Danylo Sirskyj, Ming Gong, Anne-Marie Lavoie, Gary M. Pigeau, Process development and scale-up of pluripotent stem cell manufacturing, *Cell & Gene Therapy Insights* 6 (9) (2020) 1277–1298, <https://doi.org/10.18609/cgti.2020.141>.
- [49] L. Liu, W. Michowski, A. Kolodziejczyk, P. Sicinski, The cell cycle in stem cell proliferation, pluripotency and differentiation, *Nat. Cell Biol.* 21 (2019) 1060–1067, <https://doi.org/10.1038/s41556-019-0384-4>.
- [50] K.W. Orford, D.T. Scadden, Deconstructing stem cell self-renewal: genetic insights into cell-cycle regulation, *Nat. Rev. Genet.* 9 (2008) 115–128, <https://doi.org/10.1038/nrg2269>.
- [51] D. El-Nachef, K. Shi, K.M. Beussman, R. Martinez, M.C. Regier, G.W. Everett, C. E. Murry, K.R. Stevens, J.E. Young, N.J. Sniadecki, J. Davis, A rainbow reporter tracks single cells and reveals heterogeneous cellular dynamics among pluripotent stem cells and their differentiated derivatives, *Stem Cell Rep.* 15 (2020) 226–241, <https://doi.org/10.1016/j.stemcr.2020.06.005>.
- [52] Q. Li, H. Lin, Q. Du, K. Liu, O. Wang, C. Evans, H. Christian, C. Zhang, Y. Lei, Scalable and physiologically relevant microenvironments for human pluripotent stem cell expansion and differentiation, *Biofabrication* 10 (2018), <https://doi.org/10.1088/1758-5090/aaa6b5>.
- [53] J. Wu, Y. Fan, E.S. Tzanakakis, Increased culture density is linked to decelerated proliferation, prolonged G1 phase, and enhanced propensity for differentiation of self-renewing human pluripotent stem cells, *Stem Cell. Dev.* 24 (2015) 892–903, <https://doi.org/10.1089/scd.2014.0384>.
- [54] B.S. Borys, T. Dang, T. So, L. Rohani, T. Revay, T. Walsh, M. Thompson, B. Argiropoulos, D.E. Rancourt, S. Jung, Y. Hashimura, B. Lee, M.S. Kallos, Overcoming bioprocess bottlenecks in the large-scale expansion of high-quality hiPSC aggregates in vertical-wheel stirred suspension bioreactors, *Stem Cell Res. Ther.* 12 (2021) 1–19, <https://doi.org/10.1186/s13287-020-02109-4>.
- [55] D.E.S. Nogueira, C.A.V. Rodrigues, M.S. Carvalho, C.C. Miranda, Y. Hashimura, S. Jung, B. Lee, J.M.S. Cabral, Strategies for the expansion of human induced pluripotent stem cells as aggregates in single-use Vertical-Wheel™ bioreactors, *J. Biol. Eng.* 13 (2019) 1–14, <https://doi.org/10.1186/s13036-019-0204-1>.
- [56] P. Fattahi, A. Rahimian, M.Q. Slama, K. Gwon, A.M. Gonzalez-Suarez, J. Wolf, H. Baskaran, C.D. Duffy, G. Stybayeva, Q.P. Peterson, A. Revzin, Core-shell hydrogel microcapsules enable formation of human pluripotent stem cell spheroids and their cultivation in a stirred bioreactor, *Sci. Rep.* 11 (2021) 1–13, <https://doi.org/10.1038/s41598-021-85786-2>.
- [57] I. Horiguchi, Y. Sakai, Alginate encapsulation of pluripotent stem cells using a Co-axial nozzle, *JoVE* (2015) 1–7, <https://doi.org/10.3791/52835>.
- [58] E.A. Aisenbrey, W.L. Murphy, Synthetic alternatives to matrigel, *Nat. Rev. Mater.* 5 (7) (2020) 539–551, <https://doi.org/10.1038/s41578-020-0199-8>.
- [59] S. Kaur, I. Kaur, P. Rawal, D.M. Tripathi, A. Vasudevan, Non-matrigel scaffolds for organoid cultures, *Cancer Lett.* 504 (2021) 58–66, <https://doi.org/10.1016/j.canlet.2021.01.025>.
- [60] A.M. Resto Irizarry, S. Nasr Esfahani, J. Fu, Bioengineered pluripotent stem cell models: new approaches to explore early human embryo development, *Curr. Opin. Biotechnol.* 66 (2020) 52–58, <https://doi.org/10.1016/j.copbio.2020.06.005>.
- [61] Y. Zhu, H. Wang, F. Yin, Y. Guo, F. Li, D. Gao, J. Qin, Amnion-on-a-chip: modeling human amniotic development in mid-gestation from pluripotent stem cells, *Lab Chip* 20 (2020) 3258–3268, <https://doi.org/10.1039/d0lc00268b>.
- [62] S. Hamidi, Y. Nakaya, H. Nagai, C. Alev, T. Kasukawa, S. Chhabra, R. Lee, H. Niwa, A. Warmflash, T. Shibata, G. Sheng, Mesenchymal-epithelial Transition Regulates Initiation of Pluripotency Exit before Gastrulation, *Development*, Cambridge, 2020, p. 147, <https://doi.org/10.1242/dev.184960>.
- [63] I. Barbaric, V. Biga, P.J. Gokhale, M. Jones, D. Stavish, A. Glen, D. Coca, P. W. Andrews, Time-lapse analysis of human embryonic stem cells reveals multiple bottlenecks restricting colony formation and their relief upon culture adaptation, *Stem Cell Rep.* 3 (2014) 142–155, <https://doi.org/10.1016/j.stemcr.2014.05.006>.
- [64] S. Wakao, M. Kitada, Y. Kuroda, F. Ogura, T. Murakami, A. Niwa, M. Dezawa, Morphologic and gene expression criteria for identifying human induced pluripotent stem cells, *PLoS One* 7 (2012), <https://doi.org/10.1371/journal.pone.0048677>.
- [65] M. Hashimoto, H. Sasaki, Epiblast Formation by TEAD-YAP-dependent expression of pluripotency factors and competitive elimination of unspecified cells, *Dev. Cell* 50 (2019) 139–154.e5, <https://doi.org/10.1016/j.devcel.2019.05.024>.
- [66] R. Levayer, C. Dupont, E. Moreno, Tissue crowding induces caspase-dependent competition for space, *Curr. Biol.* 26 (2016) 670–677, <https://doi.org/10.1016/j.cub.2015.12.072>.
- [67] J. Fadul, J. Rosenblatt, The forces and fates of extruding cells, *Curr. Opin. Cell Biol.* 54 (2018) 66–71, <https://doi.org/10.1016/j.cob.2018.04.007>.
- [68] E. Hannezo, C.P. Heisenberg, Mechanochemical feedback loops in development and disease, *Cell* 178 (2019) 12–25, <https://doi.org/10.1016/j.cell.2019.05.052>.
- [69] J.A. Halliwell, T.J.R. Frith, O. Laing, C.J. Price, O.J. Bower, D. Stavish, P. J. Gokhale, Z. Hewitt, S.F. El-Khamisy, I. Barbaric, P.W. Andrews, Nucleosides rescue replication-mediated genome instability of human pluripotent stem cells, *Stem Cell Rep.* 14 (2020) 1–9, <https://doi.org/10.1016/j.stemcr.2020.04.004>.
- [70] K.A. Knouse, K.E. Lopez, M. Bachofner, A. Amon, Chromosome segregation fidelity in epithelia requires tissue architecture, *Cell* 175 (2018) 200–211.e13, <https://doi.org/10.1016/j.cell.2018.07.042>.
- [71] K.L. McKinley, N. Stuurman, L.A. Royer, C. Schartner, D. Castillo-Azofeifa, M. Delling, O.D. Klein, R.D. Vale, Cellular aspect ratio and cell division mechanics underlie the patterning of cell progeny in diverse mammalian epithelia, *Elife* 7 (2018) 1–20, <https://doi.org/10.7554/eLife.36739>.
- [72] S. Singla, L.K. Iwamoto-Stohl, M. Zhu, M. Zernicka-Goetz, Autophagy-mediated apoptosis eliminates aneuploid cells in a mouse model of chromosome mosaicism, *Nat. Commun.* 11 (2020) 2958, <https://doi.org/10.1038/s41467-020-16796-3>.
- [73] E. Queleñec, C. Banal, M. Hamlin, D. Clémantine, M. Michael, N. Lefort, E. Queleñec, C. Banal, M. Hamlin, D. Clémantine, M. Michael, N. Lefort, Generation of two induced pluripotent stem cell lines IMAGINi004-A and IMAGINi005-A from healthy donors, *Stem Cell Res.* (2020), 101959, <https://doi.org/10.1016/j.scr.2020.101959>.
- [74] S.D. Sheridan, V. Surampudi, R.R. Rao, Analysis of embryoid bodies derived from human induced pluripotent stem cells as a means to assess pluripotency, *Stem Cell. Int.* (2012), <https://doi.org/10.1155/2012/738910>.
- [75] A.M. Tsankov, V. Akopian, R. Pop, S. Chetty, C.A. Gifford, L. Daheron, N. M. Tsankova, A. Meissner, A qPCR ScoreCard quantifies the differentiation potential of human pluripotent stem cells, *Nat. Biotechnol.* 33 (2015) 1182–1192, <https://doi.org/10.1038/nbt.3387>.
- [76] C. Bock, E. Kiskinis, G. Verstappen, H. Gu, G. Boulting, Z.D. Smith, M. Ziller, G. F. Croft, M.W. Amoroso, D.H. Oakley, A. Gnirke, K. Eggan, A. Meissner, Reference maps of human es and ips cell variation enable high-throughput characterization of pluripotent cell lines, *Cell* 144 (2011) 439–452, <https://doi.org/10.1016/j.cell.2010.12.032>.